RSC Advances

ROYAL SOCIETY OF CHEMISTRY

www.rsc.org/advances

Journal Name

RSCPublishing

ARTICLE

Gold Nanorods for optimized photothermal therapy: The influence of irradiating in the first and second biological window.

Cite this: DOI: 10.1039/xoxxoooooox

Received ooth January 2012,
Accepted ooth January 2012

DOI: 10.1039/xoxxoooooox

www.rsc.org/

Laura Martínez Maestro[a], Enrique Camarillo[b], José A. Sánchez Gil[c], Rogelio Rodríguez-Oliveros[d], J. Ramiro-Bargueño[e], A.J. Caamaño[e], Francisco Jaque[f], José García Solé[a] and D. Jaque[a],

The light-to-heat conversion efficiency of Gold Nanorods (GNRs) with surface plasmon resonances in the first (700-950 nm) and second (1000-1400 nm) biological windows has been studied by Quantum Dot based Fluorescence Nanothermometry. It has been found that red-shifting the GNR longitudinal surface plasmon resonance wavelength (λ_{SPR}) from the first to the second biological window is accompanied by a remarkable (close to 40%) reduction in their heating efficiency. Based on numerical simulations, we have concluded that this lower heating efficiency is caused by a reduction in the absorption efficiency (ratio between absorption and extinction cross sections). Thermal stability and ex vivo experiments have corroborated that GNRs with λ_{SPR} at around 800 nm seem to be especially suitable for efficient photothermal therapies with minimum collateral effects.

Introduction

Hyperthermia therapy (HT) consists, basically, on increasing the temperature of tissues above their normal temperature during a limited period of time. HT is nowadays emerging as an alternative treatment for a great variety of diseases. In particular, HT has been demonstrated to be especially suitable for the treatment of cancer tumors as a single-step treatment or as a co-adjuvant process for conventional treatments such as radiotherapy or chemotherapy.[1-3] The benefits of thermal therapeutics over conventional ones are numerous and include their simplicity, minimum invasivity and their potential application for the treatment of tumors allocated in vital regions where surgical resection is not feasible.[4, 5]

Traditionally, thermal therapies have employed a large variety of exciting sources to deliver heat, including laser,[6] focused ultrasound,[7] and microwave radiations.[8] Among these varieties, the use of laser sources, leading to the so-called photothermal therapies (PTTs) seems to be especially interesting. PTTs have been widely investigated as minimally invasive and highly flexible techniques. PTTs offer solutions to the limitations affecting other thermal therapies.[5] For instance, PTTs offer the possibility of eradicating tumors located nearby intrabody cavities by the use of low-loss and flexible optical fibers. However, PTTs of sub-tissue tumors non accessible by optical fibers is very restricted, due to the fact that human tissues show strong extinction coefficients in the optical range of the electromagnetic spectrum. This fact limits PTTs only to the treatment of superficial tumors. In order to overcome this limitation, PTTs must be performed by using specific excitation wavelengths at which human tissues are partially transparent, i.e. by using laser excitation wavelengths lying in the so-called biological windows (BW).[9] Traditionally, two biological windows are defined: the first Biological Window (I-BW, which extends from 700 up to 950 nm) and the second Biological Window (II-BW, 1000-1350 nm).[10, 11] Up to now, most of the reported PTTs have been carried out in the I-BW, although the continuous development of laser excitation sources in the II-BW would make treatments in this spectral range feasible in a short time.

Performing PTTs in any of the BWs would solve, partially, the penetration issue but the sole use of these spectral ranges would not provide the required selectivity, i.e. the selective heating of target tumors. This is due to the fact that both healthy and tumoral tissues show very similar absorption spectra (mainly given by water absorption bands), in such a way that a laser beam propagating into the body would heat simultaneously both tumor target and surroundings. In addition, the absorption

coefficient of tissues is typically below 0.5 cm^{-1},[12] so that the laser intensities required to achieve relevant heating by using only tissue absorptions are elevate (several W/cm^2). Both, the lack of selectivity and the requirements of large laser intensities can be simultaneously overcome by performing nanoparticle-assisted PPTs. For this purpose, nanoparticles showing large light-to-heat conversion efficiencies are selectively incorporated in cancer tumors and tissues, in such a way that, under appropriate illumination, only target tissues are efficiently heated.[13-17] Among the various heating nanoparticles that have been proposed, gold nanoparticles (GNPs) are undoubtedly the most popular ones, due to a large extent to their biocompatibility.[5, 18-22] Heating properties of gold nanoparticles are based on localized surface plasmon resonances (SPRs), which correspond to collective oscillations of conduction electrons at surface. A SPR is induced when a GNP is illuminated by an electromagnetic field at a certain wavelength, the so-called surface plasmon resonance wavelength (λ_{SPR}), whose spectral position depends on both the size and shape of GNPs. When a GNP is illuminated at λ_{SPR}, heat is generated as a consequence of the relaxation of the light excited surface currents (a process along which energy is delivered to the surrounding medium). As commented above, the spectral location of λ_{SPR} depends on the particle shape and dimensions: due to this fact it can be tuned from the visible to the near infrared by adequate tailoring of the geometrical properties of GNPs.[23] The development of fully controllable synthesis routes is leading to the development of GNPs with a great variety of geometries (nanocages, nanostars, nanoshells, and nanohexapods) that have been already demonstrated to be specially suitable for both *in vivo* and *ex vivo* PTTs.[24-29]. Despite the good results obtained with these geometries, Gold Nanorods (hereafter GNRs) have been the most studied nanoparticles for photothermal therapy purposes because of their larger infrared absorption cross section.[30] GNRs have been tested for both, *in vitro* and *in vivo* PTTs. For instance, in Kuo's work, GNRs have been successfully prepared to simultaneously serve as photodynamic therapy and hyperthermia agents with improved photodestruction efficacy and to act as an effective bioimaging probe in the NIR region [31]. GNRs offer the possibility of tailoring the λ_{SPR} in a very wide range (from visible to infrared) by just a fine adjustment of their dimensions. Indeed, it is nowadays possible to find several companies providing GNRs with λ_{SPR} varying from 700 nm up to 1100 nm, i.e. for photothermal therapies in both the I-BW and II-BW.

The light-to-heat conversion efficiency of GNRs is a key parameter for a full understanding and control of GNRs-based PPTs. Since the luminescence of GNRs is very weak (it does precise of multiphoton excitation), it is widely assumed that all the optical power absorbed by a single GNR is converted into heat. The amount of optical power that is absorbed by a single GNR is proportional to the so-called absorption efficiency Φ_{abs} that is defined as the ratio between the GNR absorption cross section (σ_{abs}) and the GNR extinction cross section ($\sigma_{ext}= \sigma_{abs} + \sigma_{scat}$, where σ_{ext} stands for the GNR extinction cross section and σ_{scat} for the scattering cross section), in such a way that $\Phi_{abs} = \sigma_{abs}/ \sigma_{ext}$. Theoretical modeling indicated that this magnitude is strongly dependent on the particular size and shape of the gold nanoparticle.[32] Although the absorption efficiency of GNRs operating in the I-BW is already known to be close to unit, [33, 34] this parameter is still unknown for GNRs with the λ_{SPR} in the II-BW. Such knowledge is essential in order to determine which spectral range (I-BW or II-BW) leads to more efficient and selective photothermal therapy based on GNRs.

In this work we report on how the absorption efficiency of commercially available GNRs is modified when the λ_{SPR} is shifted from the I-BW to the II-BW. The absorption efficiency has been experimentally determined by using quantum dot based double-beam fluorescence thermometry. This technique has been already proved to be especially suitable for the determination of absorption efficiencies of GNPs.[33-35] Experimental results are discussed and compared with theoretical predictions and numerical simulations. The obtained results have been combined with a systematic investigation of thermal stability of GNRs and with *ex vivo* experiments. Based on all these results we have elucidated on the most suitable GNRs for efficient PTTs.

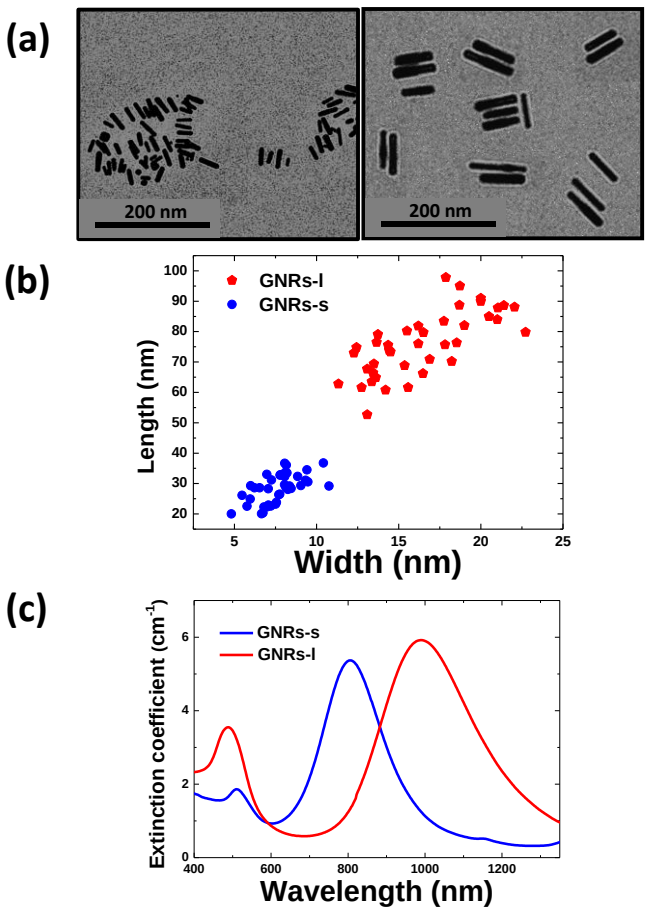

Figure 1. (a). TEM images of the two different gold nanorods provided by NanoRod Inc and investigated in this work: short gold nanorods (GNRs-s, left), long gold nanorods (GNRs-l, right). (b). Length vs Width distribution plot as obtained for the TEM images corresponding to the two kinds of GNRs. (c). Extinction spectra of the aqueous colloidal solution of the two kinds of GNRs (labeled as GNRs-s and as GNRs-l).

Experimental

Materials

The commercially available GNRs under investigation in this work were provided by Nanorods LLC. According to the manufacturer's information, these GNRs are Cetyl trimethylammonium bromide (CTAB) coated, which permits

them to be water-dispersible. We investigated two kind of GNRs: The "short" ones (GNRs-s) and the "large" ones (GNRs-l), whose Transmission Electron Microscopy (TEM) images are given in **Figure 1(a)**. From these TEM images, the size distributions of both GNRs have been estimated. The dimensions of the GNRs-s were found to be, on average, 7±2 nm width and 28±10 nm long. For the GNRs-l it was 16±7 nm width and 77±20 nm long. In **Figure 2 (b)** we have plotted the width of the GNRs versus their length. From this figure, it is clear that both kinds of GNRs have, roughly, the same aspect ratio, close to 4. These specific average dimensions were designed to have GNRs with longitudinal surface plasmon resonance in the I-BW (GNRs-s) and II-BW (GNRs-l). Indeed this is what it is really obtained, as can be seen in the extinction spectrum of both GNRS (**¡Error! No se encuentra el origen de la referencia. (c)**). This figure shows the extinction spectra of GNRs-s and GNRs-l, both dispersed in water, ($1.3x10^{11}$ nanoparticles per cm^{-3} for GNRs-s and $1.0x10^{11}$ nanoparticles per cm^{-3} for GNRs-l according to manufacturer´s specifications). For the sake of clarity, in both spectra the water absorption has been subtracted. Two extinction peaks, corresponding to the longitudinal and transversal surface plasmon resonance (SPR) modes, are observed for both kind of GNRs. Notice as the longitudinal SPR modes shift from at 808 nm for the GNRs-s to around 1000 nm for the GNRs-l; i.e. from the I-BW to the II-BW.

For the sake of comparison, we also determined the extinction spectrum of GNRs with different aspect ratios and dimensions provided by a different manufacturer (Nanopartz), and coated in a proprietary dense layer of hydrophilic polymers that shield the gold surface and give the particles ultra-long circulation times. Thus, the purpose of studying the GNRs was to get insight in to the effect of the longitudinal plasmon resonance position on the heating efficiency. As it will be shown later, the main parameter influencing the heating efficiency is the position of the longitudinal plasmon resonance regardless the particular dimension and coating of the different GNRs. We investigated up to four different kinds of GNRs with surface plasmon resonance wavelengths at 808, 900, 980 and 1090 nm with mean dimensions of 48x12, 67x12, 69x14 and 98x15 nm^2, respectively.

Quantum Dot nanothermometry.

For the purpose of fluorescence thermal sensing experiments, CdSe Quantum dots, hereafter CdSe-QDs, (Invitrogen Inc., ref Q21521MP; CA, USA) were added to the solutions containing GNRs. CdSe-QDs are well-established fluorescent probes for nanothermometry, on the basis of a linear red-shift of their emission band with increasing temperature. The temperature induced spectral shift is known to be 0.1 nm/ºC.[36] In order to avoid possible contribution of CdSe-QDs to the thermal loading of our mixed solution (CdSe-QDs+GNRs+water) we employed a very low CdSe-QDs content ($2x10^9$ nanoparticles per cubic centimeter). The mixed solution showed a very stable colloidal behavior without any evidence of precipitation during months.

Double beam fluorescence thermometry (DBFT) has been used for the determination of the absorption efficiency (Φ_{abs}), as explained elsewhere [34]. This implies the measurement of the temperature variation as a function of the heating laser power of a solution containing GNRs (acting as nanoheaters) and QDs (behaving as nanothermometers). DBFT has proven to be an adequate and reliable technique for the determination of the absorption efficiency of different heating nanoparticles.[33, 34, 37] As the fluorescence efficiency of GNRs is close to cero (in fact it is usually excited in the IR by multiphoton excitation) the absorption efficiency just gives the light to heat efficiency.[33, 34, 37, 38] In our measurements, the mixed solution was placed within a 200 µm high and 5 mm wide µ-channel (provided by Ibidi Inc.). For DBFT two counter-propagating laser beams are focused into the µ-channel at the same point. One objective (50X, 0.55 NA) was used to focus an unpolarized laser beam. This laser, tuned to the plasmon resonance wavelength of our GNRs (808 nm, or to 990 nm see **¡Error! No se encuentra el origen de la referencia. (c)**), acts as the heating laser radiation. The second objective (10X, 0.25 NA) was used to focus a 488 nm laser beam, which was spatially overlapped with the heating spot inside the sample. The 488 nm radiation was used to provide optical excitation of the CdSe-QDs (nanothermometers). The subsequently generated QDs emission was collected by the same objective and, after passing several filters and apertures, analyzed with a high-resolution spectrometer.

The on-focus temperature increase (caused by the laser induced plasmon excitation of GNRs) can be then estimated from the spectral shift induced in the CdSe-QDs emission. Previous models, concerning laser-induced thermal loading of homogeneous absorbing media, concluded that the laser-induced temperature increase at focus, ΔT_{focus}, can be written as:[39]

$$\Delta T_{focus} = \frac{P_{in}\cdot\alpha_{abs}}{2\cdot\pi\cdot K}\cdot Ln\left[\frac{D}{w_l}\right] = \frac{P_{in}\cdot\Phi_{abs}\cdot\alpha_{ext}}{2\cdot\pi\cdot K}\cdot Ln\left[\frac{D}{w_l}\right] \quad (1)$$

where K is the thermal conductivity of water (0.06 W/m·K), D is the chamber thickness (200 µm), and w_l is the laser beam waist (w_l^{808}=0.88 µm and w_l^{980}=1.07 µm), α_{abs} and α_{ext} are the absorption and extinction coefficients at the excitation wavelength and Pin is the input laser power. Thus, the on focus temperature increment normalized to the extinction coefficient ($\Delta T_f/\alpha_{ext}$) is predicted to be proportional to both the absorption efficiency and the input laser power:

$$\Delta T_f/\alpha_{ext} = \frac{\Phi_{abs}}{2\pi K}\cdot Ln(\frac{D}{w_l})\cdot P_{in} \quad (2)$$

If we denote *m* as the slope of the $\Delta T_f/\alpha_{ext}$ versus P_{in} curve ($m = \frac{d(\Delta T_f/\alpha_{ext})}{dP_l}$) then the absorption efficiency can be determined as:

$$\Phi_{abs} = m\cdot\frac{2\pi K}{Ln\left(\frac{D}{w_l}\right)} \quad (3)$$

Thermal stability experiments

In order to evaluate the potential use of GNRs as nanoheaters in photothermal treatments, the thermal stability of the nanoparticles has been investigated in the physiological temperature range. Indeed such a characterization is required as previous studies on gold nanoparticles have reported on temperature induced size and shape changes that could eventually reduce the efficacy of the undergoing photothermal treatment.[40, 41] Thus, the thermal stability of both GNRs (short and long) has been studied systematically by recording their absorption spectra after one hour annealing at different temperatures, ranging from 25 ºC up to 90 ºC (lower enough

than the boiling temperature of water). After each annealing treatment we recorded the extinction coefficient peak and the extinction wavelength. For this propose the solution containing both kinds of GNRs was placed in an Eppendorf and immersed for one hour in controlled temperature bath. After annealing, the suspension was cooled down to room temperature and its extinction spectrum measured by using a Pelkin Elmer double beam spectrophotometer.

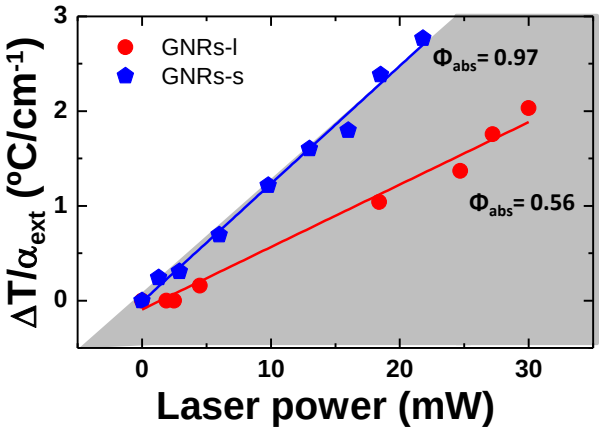

Figure 2. Laser power dependence of the on-focus temperature increase (ΔT), normalized by the extinction coefficient at the maximum wavelength ($\Delta T/\alpha_{ext}$), as obtained for the two GNRs solutions provided by NanoRod Inc. Dots are experimental data, and solid lines are the best linear fits. Shadowed area indicates the values with physical meaning, that is, those corresponding to absorption efficiencies between 0 and 1. The laser input wavelength was 800 nm for GNRs-s and 1090 nm for GNRs-l.

Experimental Results

Determination of absorption efficiency

Figure 2 shows the laser input power dependence of the $\Delta T_f/\alpha_{ext}$ ratio, as obtained for the solutions containing GNRs-s and GNRs-l when optically excited with 808 nm and 1090 nm laser beams, respectively. As can be seen, a linear relationship was observed in both cases, in agreement with **expression (2)**. This excludes the presence of possible additional laser induced phenomena, which could lead to supra-linear or sub-linear behaviors and have not been considered in the derivation of **expression (2),** such as optical trapping of GNRs and/or light induced damage of either GNRs or CdSe-QDs. The $\Delta T/\alpha_{ext}$ values with physical meaning (i.e. those that could be obtained in this laser power range for absorption efficiencies between 0 and 1), have been indicated by a shadow region in **Figure 2.**
As can be observed, all of our experimental data lie within this region revealing the correctness of our measurements. From the best linear fits (indicated by solid lines in **Figure 2**), the absorption efficiencies of both GNRs-s and GNRs-l have been obtained to be 0.97±0.03 and 0.56±0.06 for GNR-s and GNR-l, respectively. The close to unit absorption efficiency found for GNR-s is in good agreement with previous experimental results published by authors, in which GNRs with the longitudinal λ_{SPR} also close to 808 nm (manufactured by a different company, Nanopartz Inc) were used [33, 34 32, 34]. This agreement points out the fact that for GNRs with the λ_{SPR}~800 nm, the absorption of light accounts for virtually the whole optical extinction, so that scattering is almost completely negligible. The lower value of absorption efficiency obtained for GNRs-l reveals that shifting the λ_{SPR} from the I-BW to the II-BW, while keeping the aspect ratio, leads to relevant decrease in their absorption efficiency. At this point it should be noted that this reduction in the Φ_{abs} of GNRs as the λ_{SPR} is red-shifted has been also observed for other GNRs (those provided by Nanopartz Inc that have been described in **materials** section, and adjust their aspect ratios to produce longitudinal surface plasmons within the BWs). **Figure 3**. shows the absorption efficiency values obtained for different GNRs (syntetized by different companies, Nanorods LLC and NanoPartz Inc) as a function of their λ_{SPR}. This plots reveals an interesting result; independently on the particular manufacturer and on the GNRs aspect ratios, a general trend is observed; as the longitudinal λ_{SPR} shifts to larger wavelengths the absorption efficiency decreases monotonously. This fact agrees well with the previously reported tendency for metallic nanoparticles whose λ_{SPR} lied in the first biological window.[42-44] Nevertheless Figure 3 constitutes the first experimental evidence of the validity and experimental quantification of this tendency when the surface plasmon resonace is shifted from the first to the second biological window.[32]

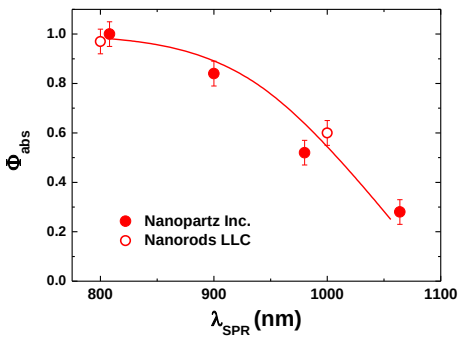

Figure 3. Absorption efficiency experimentally determined obtained for GNRs syntetized by Nanorods LLC and NanoPartz Inc displayed as a function of the corresponding surface plasmon resonance. Dots are experimental data and solid line is a guide for the eyes.

At this point, we would like to note that in the experiments included in Figure 2, the laser power densities achieved were as large as 10^4 W/cm^2. Even for such large laser power densities, the Temperature vs Laser power curve retains its linear shape. This clearly indicate that the GNRs studied in this work resulted stable even for laser power densities as large as 10^4 W/cm^2. In other words, reshaping of the GNRS studied in this work was not observed for laser power densities as large as 10^4 W/cm^2 that are much larger than typical laser power densities used in *in vivo* photothermal treatments.[45]

The agreement between our experimental data and theoretical predictions (numerical calculations) is discussed in detail in the following section.

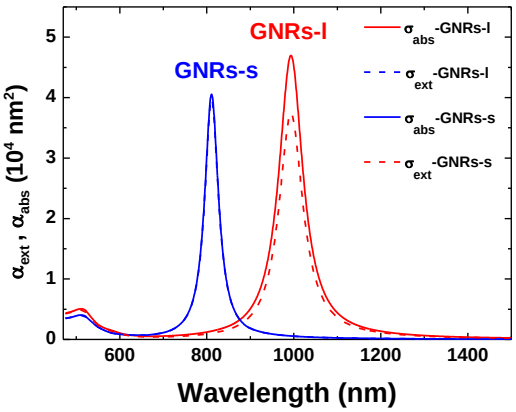

Figure 4 Calculated averaged extinction (solid curves) and absorption (dashed curves) cross sections for GNRs-s (blue curves, x10) with dimensions L=30 nm and D=7.5 nm, and for GNRs-l (red curves) with L=95 nm and D=18 nm.

Numerical calculations

In this section we proceed to give a theoretical insight into the experimental results we have reported. Thus, we focus our attention on the calculation of the optical properties of the GNRs provided by Nanorods LLC. Indeed for these GNRs the aspect ratio is fixed and they have the very same coating, CTAB; consequently the comparison of results and simulations was easier and straigthfoward. On the basis of the GNRs dimensions from the TEM images (**Figure 2**), we have calculated the extinction and absorption cross sections (σ_{ext} and σ_{abs}), so that we can compare those results with these experimentally obtained (**¡Error! No se encuentra el origen de la referencia. and 3**). To this end, full numerical calculations were carried out by means of the 3D surface integral equations (3DSIE) of the Green's Theorem method [3, 26]. The gold permittivity is obtained from Johnson and Christy measurements.[46] Since the colloidal GNRs are coated with a homogeneous CTAB molecular layer, the refractive index of the surrounding medium is not that of water (n = 1.33). Indeed, previous works have pointed that the presence of the CTAB coating induces an increase of the effective surrounding refractive index.[47-49] Based on these results, we assume that the environment refractive index is larger (*n* = n=1.435) than that of water. The simulated extinction, absorption and scattering cross sections obtained for both GNR-s and GNR-l are included in **Figure 4**.

The particular sizes used for the simulations were 7.5x30 and 18x95 nm^2 for GNR-s and GNR-l, respectively, (in accordance with the size distribution data included in **Figure 1(b),** but choosing GNRs with large volumes which in turn yield the largest contributions to the average cross sections). To reproduce the experimental conditions (unpolarized illumination on randomly oriented GNRs), four cases are considered and then averaged: illumination normal and parallel to the GNR axis, for the two linear polarizations. The resulting averaged absorption and extinction cross sections are shown in **Figure 4**. They exhibit transversal and longitudinal SPRs are consistent with the experimental extinction spectra, see **¡Error! No se encuentra el origen de la referencia. (a),** and also with our estimated environment refractive index. Regarding the spectral location of the SPRs, the transverse one appears at the same wavelength (~510 nm) for both GNRs-s and GNRs-l, in fairly good agreement with those experimentally obtained (512 nm for GNRs-s and 490 nm for GNRs-l). On the other hand, the spectral position for the longitudinal SPRs, which are the interesting ones for the purpose of this work, matches that experimentally measured for both GNRs-s and GNRs-l. From the simulations included in Figure 4, we obtained absorption efficiencies of 0.95 and 0.75 for GNRS-s and GNRs-l, respectively. Therefore, simulations reproduce well the experimentally obtained absorption efficiency of GNRs-s but overestimating that of the GNRs-l. Indeed our simulations qualitatively explains the reduction observed in the absorption efficiency as the longitudinal plasmon resonance is red-shifted (maintaining fixed the aspect ratio) but they underestimate the amount of reduction (from 0.95 to 0.75). The origin of this underestimation is not clear yet, although it could be related to size modification in the GNR-water interface thermal conductivity as it has been postulated in previous works.[50]

Thermal stability

Up to now, all the results included in this work seem to point out GNRs with λ_{SPR} in the I-BW are the most appropriate ones for photothermal therapy, as they show the largest absorption efficiencies. Nevertheless, as commented in the introduction, there is an additional point that should be considered before reach to this conclusion: the thermal resistance (or thermal stability) of the GNRs. When subjected to heating, GNRs could undergo a temperature induced shape change, due to the interplay between surface tension and partial or complete melting of gold. At this point it is not clear whether the thermal resistance of GNRs is size dependent or not; so that it is not clear whether GNRs-s shows a better thermal stability a GNRs-l or vice versa. In order to answer this open question we have performed systematic investigations on the resistance against heating cycles for both GNRs-s and GNRs-l.

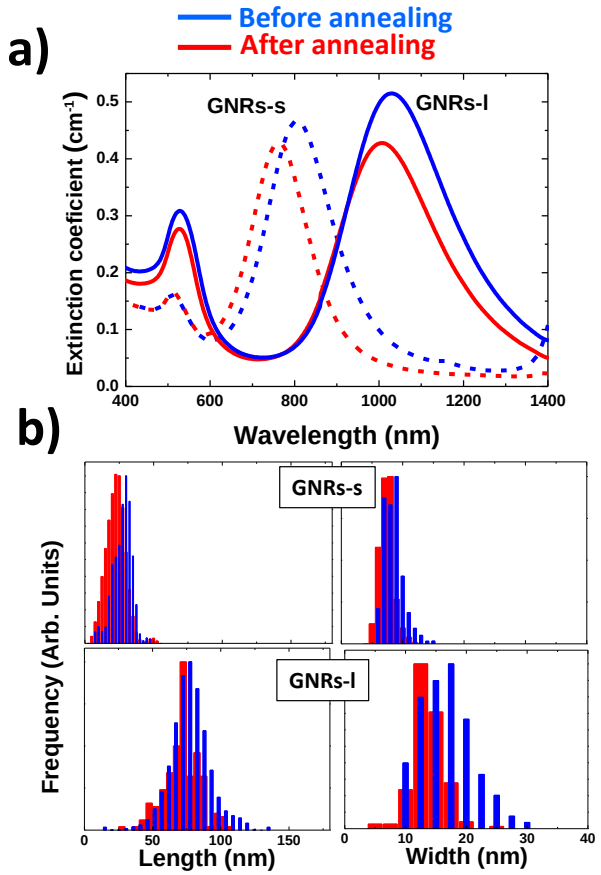

Figure 5.- (a) Extinction spectra of the aqueous colloidal solutions of short nanorods (GNRs-s) and long (GNRs-l) gold nanorods provided by NanoRod Inc. as obtained before (solid lines) and after (dashed lines) a thermal treatment up to 90 ºC for one hour.(b) Size histograms as obtained before and after thermal treatments. TEM images used to get this histograms can be found in the supplementary information.

Figure 5 (a) displays the room temperature extinction spectra of the aqueous colloidal solutions of GNRs-s and GNRs-l before and after annealing at 90 ºC for one hour. As can be observed, in both cases the longitudinal SPR peak of the both GNRs suffers a blue shift that is accompanied by a slight reduction in the peak extinction coefficient. The observed blue shift reveals shape changes ("reshaping") as a consequence of thermal annealing. Such shape changes have been corroborated by TEM measurements. These TEM measurements have revealed that the average dimensions of GNRs-s (GNR-l) are reduced from 7x28 nm^2 (16x77 nm^2) down to 8x22 nm^2 (13x72 nm^2), as a can be observed from the size histograms included in Figure 5(b). Thus thermal annealing has produced in both cases a reduction in the GNR aspect ratio close to 10%. This reduction in the aspect ratio explains well the observed blue shift of the GNRs. Indeed, as reported by many authors[51, 52], the surface plasmon resonance wavelength increases with the GNR aspect ratio. It is important to note here that the temperature induced blueshift of λ_{SPR} has been induced for both GNRs-s and GNRs-l only when the annealing temperature reaches a certain value (about 70ºC), as observed in **Figure 6.** This figure shows the spectral position of the longitudinal SPR as a function of annealing temperature, as obtained for both types of GNRs. As can be observed remarkable changes were only induced in both cases for annealing temperatures above 70ºC. Experimental data included in **Figure 6** have been found in excellent agreement with previous works. Indeed, Carbó-Argibay et al., also reported on strong modification of the optical and morphological properties of GNRs dispersed in N,N-Dimethylformamide (DMF) when they were subjected to annealing treatments above 70 ºC. [51, 52] The fact that the minimum temperature required for the modification of the optical properties of GNRs does not depend on the GNR dimensions, points out the fact that this critical temperature is very likely related not to the mechanical properties of the GNRs but to their specific CTAB coating.

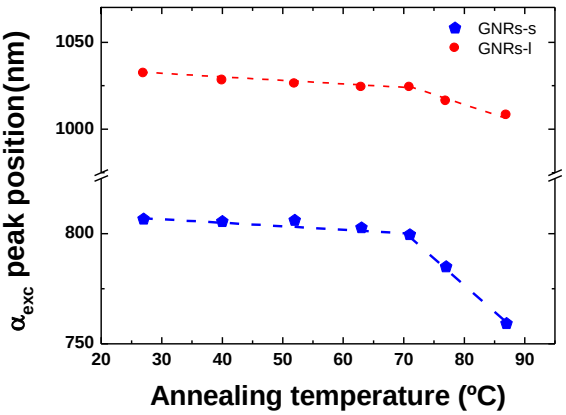

Figure 6.- Spectral position of the surface plasmon resonance of both GNRs-s and GNRs-l as obtained after one hour thermal treatments at different tempereatures ranging from 25 up to 89 ºC. Dots are experimental data and solid lines are guides for the eyes.

Ex vivo experiments.

For real *in vivo* photothermal treatments the suitability and potential use of a given type of GNRs would not only depend on their light-to-heat conversion efficiency but also on the overlap between the GNR and tissue extinction spectra. If there is a spectral overlap between tissue and GNR extinction spectra, the laser radiation used for optical excitation of GNRs would also be partially absorbed by the tissue. Therefore, the light induced heating would not be selective, as it is not only produced at the GNR location. At the same time, optical scattering along the tissue would lead to a reduction in the sub-tissue laser excitation intensity and, thus, to a less effective photothermal treatment. Therefore, the optimum excitation wavelength would be based not only on the heating efficiency of the GNRs, but also by the interplay between the wavelength dependence of tissue extinction (i.e. absorption and scattering). Generally speaking, tissue absorption is minimized in the I-BW, whereas optical scattering is minimized in the II-BW.[37, 53, 54] In order to elucidate how this interplay affects the potential use of GNRs for photothermal therapies, we have performed *ex vivo* experiments with the two kinds of GNRs under study in

this work. **¡Error! No se encuentra el origen de la referencia.** shows side-view thermal images of chicken breast tissues subcutaneously injected with 5 µl ($1.0x10^{11}$ nanoparticles per cm^{-3}) of GNRs-l (left) and GNRs-s (right), as obtained when illuminating with $1W/cm^2$ laser beams at 808 and 1090 nm, respectively. Arrows in **Figure 7** indicate the beam paths of both lasers. In all cases, the maximum tissue temperature is induced at the location of GNR injection. However, for the case of 1090 nm, irradiation tissue heating spreads out to the surrounding tissue due to the non-vanishing absorption coefficient of tissues at this wavelength. On the contrary, for GNRs-s (excited at 808 nm), tissue heating is essentially limited to the injection area, and so, the heating is highly selective. Consequently, from the point of view of treatment selectivity, GNRs operating in the first biological window (i.e. GNRs-s) seem to be also more advantageous than those operating in the second biological window (i.e. GNRs-l).

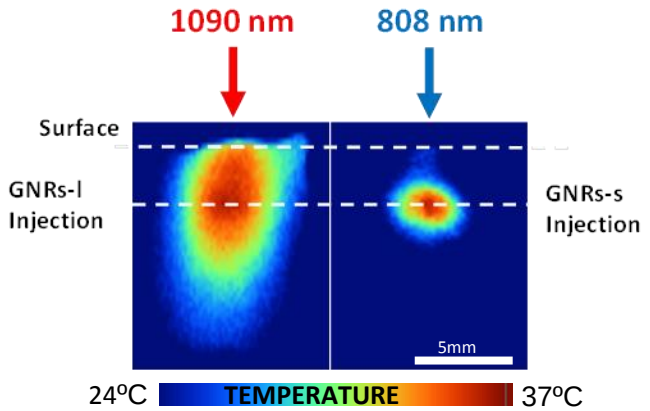

Figure 7.- Steady state infrared thermal images of chicken breasts under 1 W/cm2 laser irradiation at 808 and 1090 nm in the presence of a sub-tissue injection of GNRs-s and GNRs-l, respectively. The location of tissue surface and the injection are schematically indicated by dashed lines. Arrows indicate the laser beam path.

Conclusions

In summary, quantum dot fluorescence nanothermometry measurements have led to the conclusion that the heating efficiency of commercially available GNRs, with longitudinal surface plasmon resonance close to 808 nm (i.e., lying within the first bio-window) is almost 40% higher than that of GNRs with larger dimensions and a surface plasmon resonance around 1000 nm, (i.e., lying in the second biological window). From systematic investigations on different GNRs with variable length and width size, it has been found that the absorption efficiency depends on the surface plasmon resonance with almost independence of both the particular GNRs dimension and coating. A general trend has been obtained, so that the heating efficiency is monotonously dependent with increasing longitudinal surface plasmon resonance. Additional experiments concerning the thermal stability of GNRs and the spatial selectivity of GNRs (based on *ex vivo* photothermal treatments) pointed out that GNRs working in the first biological window (with surface plasmon resonances around to 800 nm) are the optimum ones for photothermal therapy. Thus, the results here reported open new opportunities for further optimization of photothermal therapies based on gold nanorods.

Acknowledgements

This work was supported by the Universidad Autónoma de Madrid and Comunidad Autónoma de Madrid (Project S2009/ MAT-1756 and S2009/TIC1476), by the Spanish Ministerio de Educacion y Ciencia (MAT2010-16161 and MAT2010-21270-C04-02, FIS2012-31070 and Consolider-Ingenio EMET CSD2008-00066) L.M.M thanks the Spanish Ministerio de Economia y competitividad (MINECO) for a FPI grant.

Notes and references

[a] Fluorescence Imaging Group, Departamento de Física de Materiales, Instituto Nicolás Cabrera, Facultad de Ciencias, Universidad Autónoma de Madrid, 28049 Spain.
[b] Universidad Autónoma de México, México DF.
[c] Instituto de Estructura de la Materia (IEM-CSIC), Consejo Superior de Investigaciones Científicas, Serrano 121, 28026 Madrid (Spain)..
[d] Institut fur Physik, Humboldt-Universitat zu Berlin Newtonstr. 15, 12489 Berlin (Germany).
[e] Department of Signal Theory and Communication, School of Telecommunication Engineering, Universidad Rey Juan Carlos, Madrid 28943, Spain.
[f] Departamento de Biología, Universidad Autónoma de Madrid, 28049 Spain.

1. R. W. Habash, R. Bansal, D. Krewski and H. T. Alhafid, *Crit Rev Biomed Eng*, 2006, **34**, 459-489.
2. R. W. Habash, R. Bansal, D. Krewski and H. T. Alhafid, *Crit Rev Biomed Eng*, 2006, **34**, 491-542.
3. R. Rodríguez-Oliveros and J. A. Sánchez-Gil, *Opt. Express*, 2012, **20**, 621-626.
4. W. R. Chen, R. L. Adams, R. Carubelli and R. E. Nordquist, *Cancer Lett*, 1997, **115**, 25-30.
5. D. P. O'Neal, L. R. Hirsch, N. J. Halas, J. D. Payne and J. L. West, *Cancer Lett*, 2004, **209**, 171-176.
6. I. H. El-Sayed, X. Huang and M. A. El-Sayed, *Cancer Lett*, 2006, **239**, 129-135.
7. J. B. Marmor, D. Pounds, T. B. Postic and G. M. Hahn, *Cancer*, 1979, **43**, 188-197.
8. J. Mendecki, E. Friedenthal, C. Botstein, R. Paglione and F. Sterzer, *International journal of radiation oncology, biology, physics*, 1980, **6**, 1583-1588.
9. R. Weissleder, *Nat Biotechnol*, 2001, **19**, 316-317.
10. K. Konig, *J Microsc*, 2000, **200**, 83-104.
11. A. M. Smith, M. C. Mancini and S. Nie, *Nat Nanotechnol*, 2009, **4**, 710-711.
12. G. Marquez, L. V. Wang, S. P. Lin, J. A. Schwartz and S. L. Thomsen, *Appl Opt*, 1998, **37**, 798-804.

13. L. Bickford, J. Sun, K. Fu, N. Lewinski, V. Nammalvar, J. Chang and R. Drezek, *Nanotechnology*, 2008, **19**, 315102.
14. J. V. Frangioni, *Journal of clinical oncology : official journal of the American Society of Clinical Oncology*, 2008, **26**, 4012-4021.
15. X. Huang, I. H. El-Sayed, W. Qian and M. A. El-Sayed, *J Am Chem Soc*, 2006, **128**, 2115-2120.
16. Z. Liu, F. Kiessling and J. Gätjens, *Journal of Nanomaterials*, 2010, **2010**, 1-15.
17. C. Loo, A. Lin, L. Hirsch, M. H. Lee, J. Barton, N. Halas, J. West and R. Drezek, *Technol Cancer Res Treat*, 2004, **3**, 33-40.
18. W. Cai, T. Gao, H. Hong and J. Sun, *Nanotechnol., Sci. Appl.*, 2008, **1**, 17–32.
19. X. Huang, P. K. Jain, I. H. El-Sayed and M. A. El-Sayed, *Lasers in Medical Science*, 2008, **23**, 217-228.
20. M. Marsh, E. Schelew, S. Wolf and T. Skippon, *Queen's University, Kingston*, 2009, **29**.
21. D. Pissuwan, S. M. Valenzuela and M. B. Cortie, *Trends Biotechnol*, 2006, **24**, 62-67.
22. M. L. Debasu, D. Ananias, I. Pastoriza-Santos, L. M. Liz-Marzán, J. Rocha and L. D. Carlos, *Advanced Materials*, 2013, **25**, 4817-4817.
23. G. Baffou, R. Quidant and C. Girard, *Applied Physics Letters*, 2009, **94**, 153109.
24. J. Chen, C. Glaus, R. Laforest, Q. Zhang, M. Yang, M. Gidding, M. J. Welch and Y. Xia, *Small*, 2010, **6**, 811-817.
25. H. Yuan, C. G. Khoury, C. M. Wilson, G. A. Grant, A. J. Bennett and T. Vo-Dinh, *Nanomedicine*, 2012, **8**, 1355-1363.
26. R. Rodriguez-Oliveros and J. A. Sanchez-Gil, *Opt Express*, 2011, **19**, 12208-12219.
27. Y. Wang, K. C. Black, H. Luehmann, W. Li, Y. Zhang, X. Cai, D. Wan, S. Y. Liu, M. Li, P. Kim, Z. Y. Li, L. V. Wang, Y. Liu and Y. Xia, *ACS Nano*, 2013, **7**, 2068-2077.
28. D. Bartczak, O. L. Muskens, S. Nitti, T. Sanchez-Elsner, T. M. Millar and A. G. Kanaras, *Small*, 2012, **8**, 122-130.
29. J. L. Li, D. Day and M. Gu, *Advanced Materials*, 2008, **20**, 3866-3871.
30. T. B. Huff, L. Tong, Y. Zhao, M. N. Hansen, J. X. Cheng and A. Wei, *Nanomedicine (Lond)*, 2007, **2**, 125-132.
31. W. S. Kuo, C. N. Chang, Y. T. Chang, M. H. Yang, Y. H. Chien, S. J. Chen and C. S. Yeh, *Angew Chem Int Ed Engl*, 2010, **49**, 2711-2715.
32. P. K. Jain, K. S. Lee, I. H. El-Sayed and M. A. El-Sayed, *J Phys Chem B*, 2006, **110**, 7238-7248.
33. L. M. Maestro, P. Haro-Gonzalez, A. Sanchez-Iglesias, L. M. Liz-Marzan, J. Garcia Sole and D. Jaque, *Langmuir*, 2014, **30**, 1650-1658.
34. L. M. Maestro, P. Haro-Gonzalez, J. G. Coello and D. Jaque, *Applied Physics Letters*, 2012, **100**, 201110.
35. L. M. Maestro, P. Haro-Gonzalez, M. C. Iglesias-de la Cruz, F. Sanz-Rodriguez, A. Juarranz, J. G. Sole and D. Jaque, *Nanomedicine (Lond)*, 2013, **8**, 379-388.
36. L. M. Maestro, E. M. Rodriguez, F. S. Rodriguez, M. C. la Cruz, A. Juarranz, R. Naccache, F. Vetrone, D. Jaque, J. A. Capobianco and J. G. Sole, *Nano Lett*, 2010, **10**, 5109-5115.
37. L. M. Maestro, P. Haro-Gonzalez, B. del Rosal, J. Ramiro, A. J. Caamano, E. Carrasco, A. Juarranz, F. Sanz-Rodriguez, J. G. Sole and D. Jaque, *Nanoscale*, 2013, **5**, 7882-7889.
38. L. M. Maestro, E. M. Rodriguez, F. Vetrone, R. Naccache, H. L. Ramirez, D. Jaque, J. A. Capobianco and J. G. Sole, *Opt Express*, 2010, **18**, 23544-23553.
39. H. Mao, J. R. Arias-Gonzalez, S. B. Smith, I. Tinoco, Jr. and C. Bustamante, *Biophys J*, 2005, **89**, 1308-1316.
40. C. Kan, X. Zhu and G. Wang, *J Phys Chem B*, 2006, **110**, 4651-4656.
41. M. B. Mohamed, Z. L. Wang and M. A. El-Sayed, *The Journal of Physical Chemistry A*, 1999, **103**, 10255-10259.
42. H. Chen, L. Shao, T. Ming, Z. Sun, C. Zhao, B. Yang and J. Wang, *Small*, 2010, **6**, 2272-2280.
43. M. A. Mackey, M. R. K. Ali, L. A. Austin, R. D. Near and M. A. El-Sayed, *The Journal of Physical Chemistry B*, 2014, **118**, 1319-1326.
44. K. Jiang, D. A. Smith and A. Pinchuk, *The Journal of Physical Chemistry C*, 2013, **117**, 27073-27080.
45. D. Jaque, L. Martínez Maestro, B. Del Rosal, P. Haro-Gonzalez, A. Benayas, J. L. Plaza, E. Martín Rodríguez and J. García Solé, *Nanoscale*, 2014, **6**, 9494-9530.
46. P. B. Johnson and R. W. Christy, *Physical Review B*, 1972, **6**, 4370-4379.
47. C. J. Murphy, T. K. Sau, A. M. Gole, C. J. Orendorff, J. Gao, L. Gou, S. E. Hunyadi and T. Li, *The Journal of Physical Chemistry B*, 2005, **109**, 13857-13870.
48. C. Yu, L. Varghese and J. Irudayaraj, *Langmuir*, 2007, **23**, 9114-9119.
49. H. Chen, X. Kou, Z. Yang, W. Ni and J. Wang, *Langmuir*, 2008, **24**, 5233-5237.
50. G. Baffou, R. Quidant and C. Girard, *Physical Review B*, 2010, **82**, 165424.
51. E. Carbó-Argibay, B. Rodríguez-González, J. Pacifico, I. Pastoriza-Santos, J. Pérez-Juste and L. M. Liz-Marzán, *Angewandte Chemie International Edition*, 2007, **46**, 8983-8987.
52. H. Petrova, J. Perez Juste, I. Pastoriza-Santos, G. V. Hartland, L. M. Liz-Marzan and P. Mulvaney, *Physical chemistry chemical physics : PCCP*, 2006, **8**, 814-821.
53. C. Xu, W. Zipfel, J. B. Shear, R. M. Williams and W. W. Webb, *Proceedings of the National Academy of Sciences of the United States of America*, 1996, **93**, 10763-10768.
54. M. F. Tsai, S. H. Chang, F. Y. Cheng, V. Shanmugam, Y. S. Cheng, C. H. Su and C. S. Yeh, *ACS Nano*, 2013, **7**, 5330-5342.

